APPENDIX B

Publication P2

Repo A.-K., Arkkio A. Numerical impulse response test to estimate circuit-model parameters for induction machines. *IEE Proceedings – Electric Power Applications*, Vol. 153, No. 6, November 2006, pp. 883-890.

Numerical impulse response test to estimate circuit-model parameters for induction machines

A. Repo and A. Arkkio

Abstract: The estimation of electrical parameters of a cage induction machine is studied. First, the steady-state parameters are estimated using two-dimensional finite element analysis (FEA) with the assumption of sinusoidal time variation. Next, a numerical impulse response test using time-stepping FEA is utilised to produce the voltage–current data for the small-signal model parameter estimation. The method is based on the assumption of linear behaviour near the operating point and the choice for the suitable excitation signal is studied. To distinguish the influence of the skin effect, the impulse response test is also performed for the corresponding slip-ring machine. The parameters are estimated from the frequency response function of the stator line current using differential evolution. The results of the FE simulations are compared with measurements.

1 Introduction

Time-stepping finite-element analysis (FEA) is an accurate and widely applied method in the study and simulation of electrical machines. With the numerical magnetic field analysis, features that can be difficult, expensive or even impossible to measure can be explored. On the other hand, electrical machines usually operate in connection with control circuits, power electronics, components of electrical grid and mechanics causing a complex interaction. The computation capacity often limits the use of comprehensive models and a simpler analytical model for the machine is required in many applications.

The purpose of this work is to study whether the accurate information on the machine behaviour provided by the numerical field solution can be compressed into the form of an analytical model. This is done by estimating the parameters of the analytical model using the simulation data provided by the finite-element analysis. For estimation of the parameters of the equivalent circuit, the voltage–current model is the most straightforward approach. Several papers have been presented on estimating the parameters by fitting a voltage–current model to measured data [1–3]. In sensorless control of induction machines, the signal injection is widely applied in the estimation of the parameters and rotor speed [4–6]. When modelling the electrical machine within the FEA, the steady-state parameters are derived from the time harmonic field solution. In [7–10], the parameters are derived supplying the stator and rotor conductors in turn and solving the induced magnetic field. In [11, 12], the basic circuit parameters are obtained from the simulated no-load and locked-rotor tests. In [8] and [13], the transient behaviour of the machine is modelled using dynamic inductances, which are calculated within the time-stepping FEA.

IEE Proceedings online no. 20060047

doi:10.1049/ip-epa:20060047

Paper first received 7th February and in final revised form 10th May 2006

The authors are with the Laboratory of Electromechanics, PO Box 3000, FI-02015 TKK, Finland

E-mail: anna-kaisa.repo@tkk.fi

The starting point of this work is the impulse method introduced by Tenhunen [14] and expanded by Holopainen [15]. The time-consuming forced whirling method was replaced by an impulse test providing data from a wide frequency range for identification of a parametric force model. The impulse excitation was applied to the displacement of the rotor, and from the response of the force acting between the eccentric rotor and stator, the parameters of the force model could be estimated. In the case of the force model, the impulse method has given good results and the idea of expanding the use of it has arisen.

An electrical machine is a highly nonlinear system and, if the impulse method is applied, it is assumed that the system can be linearised in the neighbourhood of some operating point. In the case of a voltage–current model, this means that, for small perturbations in the voltage, the response of the current can be approximated with a linear model. In the frequency domain, every frequency in the input should excite the system only at that same frequency. In the case of the force model, the frequency responses of the forced whirling method and the impulse method coincide well, indicating the linearity of the system. Corresponding to the forced whirling method, a continuous sinusoidal signal, referred to as harmonic excitation, is added to the stator voltage supply. The frequency response function (FRF) is also measured using harmonic excitation.

An incremental magnetic field excited by a voltage or current impulse faces an incremental permeability of the nonlinear core. The parameters of the small-signal model are related to the incremental permeability. In the steady state, the RMS currents, fluxes and voltages and the related circuit parameters are associated with the effective permeability [16]. Harmonic analysis is used for estimating the steady-state parameters and those are also defined by measurements. The small-signal model parameters are noted with lower-case letters and the steady-state parameters with capital letters.

2 Analytical models

2.1 Stator current model

For estimation of the electrical parameters of the equivalent circuit, the most straightforward approach is to use a

voltage–current model The voltage and flux-linkage equations for an induction machine in the stator reference frame are defined by (1)–(4):

$$\underline{u}_s^s = R_s \underline{i}_s^s + \frac{d\underline{\psi}_s^s}{dt} \tag{1}$$

$$\underline{u}_r^s = R_r \underline{i}_r^s + \frac{d\underline{\psi}_r^s}{dt} - j\omega \underline{\psi}_r^s \tag{2}$$

$$\underline{\psi}_s^s = L_s \underline{i}_s^s + L_m \underline{i}_r^s \tag{3}$$

$$\underline{\psi}_r^s = L_m \underline{i}_s^s + L_r \underline{i}_r^s \tag{4}$$

To use currents as variables, the flux equations (3) and (4) are substituted into the voltage (1) and (2). The rotor current is eliminated substituting equations (2) into (1). The small-signal model at a constant speed is obtained by applying a small disturbance to the steady-state stator voltage and current and subtracting the steady-state from the disturbed state. The FRF of the stator current (5) is obtained by assuming the initial values to be zero and replacing the time derivatives with multiplication by $j\omega$. The small-signal parameters are denoted by lower-case letters:

$$\frac{\Delta \underline{i}_s(j\omega)}{\Delta \underline{u}_s(j\omega)} = \frac{j\omega l_r - j\omega_0 l_r + r_r}{\omega^2\left(l_m^2 - l_s l_r\right) + \omega(j r_s l_r + j r_r l_s + \omega_0 l_s l_r - \omega_0 l_m^2) + r_s r_r - j\omega_0 r_s l_r} \tag{5}$$

The parameters are the stator resistance r_s, rotor resistance r_r, magnetising inductance l_m, stator leakage inductance $l_{\sigma s}$ and rotor leakage inductance $l_{\sigma r}$. The stator and rotor self inductances l_s and l_r are sums of the magnetising inductance and the corresponding leakage inductance. In this work, this voltage–current model is used as a physical model fitted to the simulated frequency response data.

2.2 More advanced current–voltage models

The induction machine model derived from the space-vector theory with physically meaningful parameters is sufficient in many applications. However, model (5) does not include all the features presented by FEA, such as the saturation and the skin effect in the rotor bars. Smith *et al.* [17] have proposed a more advanced state-space model, which takes into account the skin effect. In the model, one or more additional rotor branches are included in the basic equivalent circuit when the rotor currents of the new branches act as additional state variables. A more complex rotor model has been proposed by Sudhoff *et al.* [18]. The steady-state equivalent circuit is modified by replacing the rotor impedance with a transfer function, the order and coefficients of which are estimated from a measured frequency response.

3 Methods for parameter estimation

A 37 kW cage-induction motor with closed rotor slots is studied. The rated values are given in Table 1 and the shape of the rotor and stator slots are shown in Fig. 1. The estimation methods are based on two-dimensional FEA, where the effects of the end-rings and stator end windings are taken into account by the end resistances and inductances. The details of the methods are given in [9]. The finite-element mesh consists of 1516 second-order triangular elements. The rotor is unskewed. In the simulations, the temperature of the stator windings is 98°C and rotor cage 135°C. The stator resistance given to the FE model is 0.083573 Ω.

Table 1: Rated values of 37 kW cage induction motor

P_N [kW]	rated power	37
U_{sN} [V]	rated stator voltage	380 (star)
p	number of pole pairs	2
f_N [Hz]	rated stator frequency	50
s_N [%]	rated slip	2.0

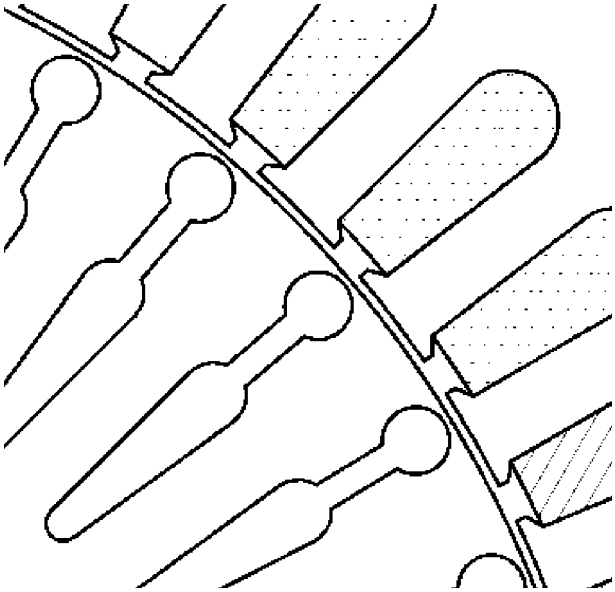

Fig. 1 *Cross-sectional geometry of rotor and stator slots*

3.1 Impedance method

In the case of magnetically linear material and steady-state condition, the time dependence can be eliminated using phasor variables. The assumption does not hold for nonlinear materials or when the rotor is rotating but it is often used to simplify the problem. The method utilising harmonic analysis is referred to later on as the impedance method.

Arkkio [9] has applied the concept of the impedance matrix [7] to derive the steady-state parameters of the equivalent circuit. The impedance matrix defines the relation between potential differences and currents, and when the potential difference is known, the impedance matrix and the current vector can be found iteratively. The reluctances of the elements given by the nonlinear field solution are fixed in order to separate the couplings between the windings. The impedance matrix is constructed supplying a current to one stator phase or rotor bar at a time and solving the magnetic field for the linearised material. The parameters of the equivalent circuit can be calculated from the components of the impedance matrix taking into account reference of rotor quantities to the stator.

3.2 Impulse response test and harmonic excitation

In this work, the impulse test is performed numerically within a 2D time-stepping finite-element analysis, which includes the magnetic saturation, skin effect in the rotor bars and rotation of the rotor. The impulse test is carried out as follows. At the beginning of the test, the electrical machine is in the steady state. The impulse excitation is added to the steady-state line-to-line

voltage vector v_s:

$$\underline{v}_s + \Delta\underline{v}_s = |\underline{v}_s|e^{j\omega_s t} + |\Delta\underline{v}_s(t)|e^{j(\omega t+\alpha)} \quad (6)$$

where ω_s is the angular supply frequency, and ω and α are the angular frequency and phase angle of the impulse. In the simulations, both ω and α are chosen to be zero. With these assumptions the disturbed line-to-line stator voltage $v_{bc} + \Delta v_{bc}$, for example, is

$$\begin{aligned} v_{bc} + \Delta v_{bc} &= \hat{v}\cos\left(\omega_s t - \frac{2\pi}{3}\right) + |\Delta\underline{v}_s(t)|\cos\left(-\frac{2\pi}{3}\right) \\ &= \hat{v}\cos\left(\omega_s t - \frac{2\pi}{3}\right) - \frac{1}{2}|\Delta\underline{v}_s(t)| \end{aligned} \quad (7)$$

Two different types of voltage impulses are tested. The amplitudes of the voltage impulse are defined by (8) (voltage impulse 1) and (9) (voltage impulse 2):

$$|\Delta\underline{v}_s(t)| = \begin{cases} a_{\text{rel}}\hat{v}\sin^2(2\pi f_d t), & t_1 \le t \le t_1 + t_d \\ 0, & \text{otherwise} \end{cases} \quad (8)$$

$$|\Delta\underline{v}_s(t)| = \begin{cases} a_{\text{rel}}\hat{v}\sin^3(4\pi f_d t) + ca_{\text{rel}}\hat{v}\sin^2(2\pi f_d t), & t_1 \le t \le t_1 + t_d \\ 0, & \text{otherwise} \end{cases} \quad (9)$$

where $\hat{v}$ is the amplitude of the steady-state line-to-line voltage and t_1 is the time step at the beginning of the impulse. The relative amplitude a_{rel} and the line-to-line voltage define the magnitude, and the frequency f_d and duration time t_d define the frequency contents of the impulse [19].

The time step of the FE analysis is 50 μs and the total number of time steps is 40 000 in order to obtain a frequency resolution of 0.5 Hz without any zero padding. The impulse test is performed twice with both a positive and a negative amplitude a_{rel} using the same initial steady state. The impulse excitations and corresponding responses obtained are subtracted from each other in order to cancel the frequencies that are naturally produced by the electrical machine in its normal operation. Since model (5) is derived for the phase variables, $\Delta\underline{u}_s$ is computed from the voltages across the stator phase windings and $\Delta\underline{i}_s$ from the phase currents. These are transformed to the frequency domain using FFT and from the ratio the FRF of the stator current is obtained.

The impulse has to excite all the frequencies within the frequency range studied. The length of the impulse defines the frequency range in which the frequency content is nonzero. If f_d is 100 Hz and t_d is 5 ms, the frequency content of voltage impulse 1 is nonzero between -400 and 400 Hz. The maximum amplitude is in the middle of the impulse in the time domain and at DC in the frequency domain. The first term of voltage impulse 2 has maxima at -200 and 200 Hz, where the gain for the current is already quite low. The nonzero frequency range is also -400 to 400 Hz, except at DC where the frequency content is zero. This is corrected with a second term similar to impulse 1 but with amplitude multiplied by coefficient c.

The magnitude of the impulse has to be small enough to produce a linear response. On the other hand, very small amplitudes may cause problems with numerical accuracy. Here, the relative amplitudes a_{rel} of 0.05, 0.1 and 0.15 were tested for voltage impulse 1. For voltage impulse 2, a_{rel} was 0.05 and the coefficient c was varied between 0.01 and 0.1. Figures 2 and 3 show the frequency contents of Δu_s with voltage impulses 1 and 2, when a_{rel} is 0.05 and c is 0.02.

The FRF can also be produced frequency by frequency using the harmonic excitation. The additional frequency

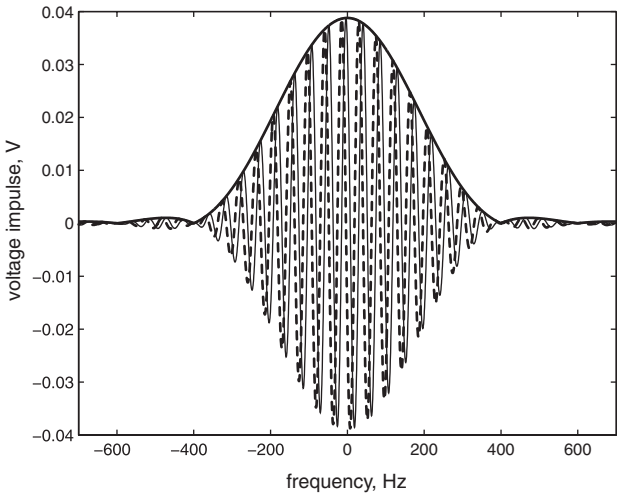

Fig. 2 *Frequency content of voltage impulse 1*

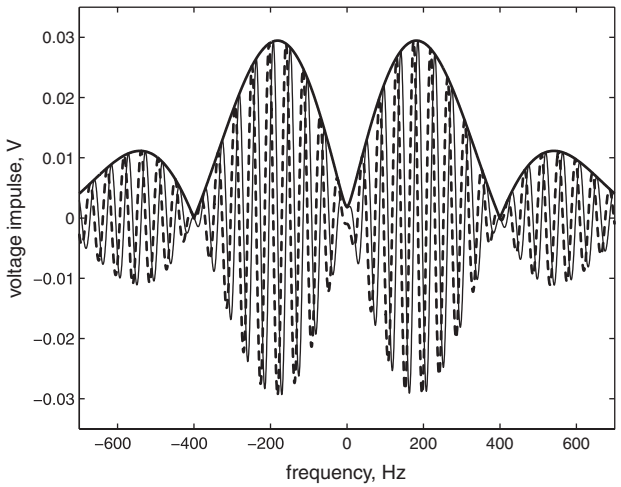

Fig. 3 *Frequency content of voltage impulse 2*

peaks caused by saturation can be neglected and therefore the obtained FRF is considered as an ideal FRF. The test is performed replacing the impulse with a continuous sinusoidal signal:

$$\Delta\underline{v}_s = a_{\text{rel}}\hat{v}e^{j(\omega t+\alpha)} \quad (10)$$

The influence of the impulse phase angle α was studied using the harmonic excitation at frequencies 15 and 25 Hz. When α was varied between 0 and 90°, the difference between the FRFs was found to be less than 0.01%.

Figure 4 slows the FRF of the current produced by voltage impulse 1. It gives the highest energy at low frequencies where the current gain is high owing to the small stator resistance. The low-frequency current component causes saturation, which can be detected as additional peaks in the frequency region 50–100 Hz and around -200 Hz. Decreasing a_{rel} to 0.01 does not improve the shape of the FRF significantly.

Figure 5 shows the FRF produced by voltage impulse 2 compared with the single frequency points simulated by harmonic excitation. When using voltage impulse 2, the amplitude of the impulse at low frequencies is reduced. When c is between 0.05 and 0.1, low additional peaks in the frequency range 50–100 Hz are still detected. With $c = 0.01$, the denominator is close to zero at DC. Choosing $c = 0.02$ is a compromise that gives a relatively good result. The FRFs from the harmonic and impulse excitations differ mostly in

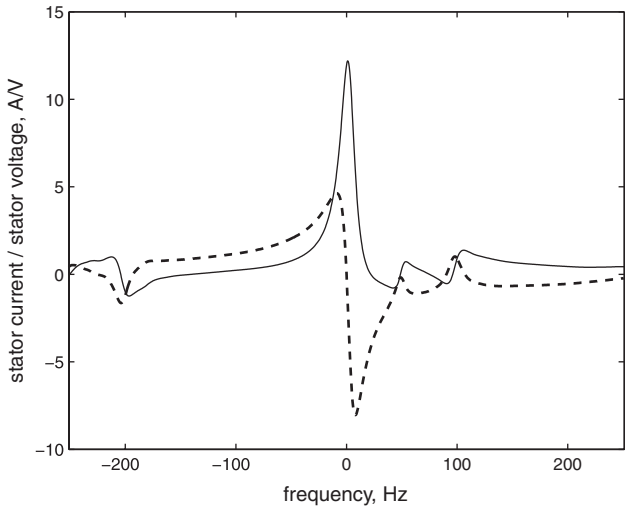

Fig. 4 *FRF calculated by impulse response test using voltage impulse 1*

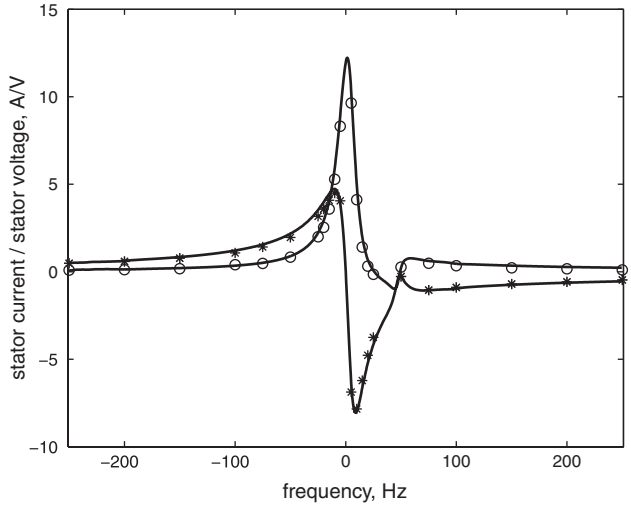

Fig. 5 *FRFs calculated by impulse response test using voltage impulse 2 (line) and harmonic excitation*
○ real part
* imaginary

the range − 25 and 0 Hz. For an electrical machine, the iron parts are saturated at the rated load and some additional frequency peaks can be expected to appear in the current response. Also, the motion of the rotor causes dispersion of the frequencies.

If the machine is supplied from a current source, the impulse can be added to the stator current:

$$|\Delta \underline{i}_s(t)| = \begin{cases} a_{\text{rel}}\hat{i}\sin^2(2\pi f_d t), & t_1 \le t \le t_1 + t_d \\ 0, & \text{otherwise} \end{cases} \quad (11)$$

where $\hat{i}$ is the amplitude of the steady-state line current. For the current impulse, relative amplitudes within the range 0.01–0.3 are applied. Changing the amplitude shifts the curves mostly in the range − 20 to 20 Hz but the maximum difference is only 4%. The general shape of the FRF is very close to the FRF simulated using voltage impulse 2 (Fig. 5), which is chosen for the parameter estimation.

3.3 Skin effect with modified FE model

Besides the saturation, model (5) with constant parameters cannot include the skin effect, which can be especially significant with this rotor slot shape (Fig. 1). To study the skin effect, the FE model for a slip-ring machine is built by replacing the rotor bars of the cage-induction model with thin conductors. With zero rotor voltage, this model corresponds to the cage-induction machine omitting the skin effect in the rotor bars. The effect of saturation can be removed by replacing the nonlinear materials of the FE models with linear ones.

The only difference between the two linearised FE models is that, in the case of the slip-ring machine, the current density is constant in the cross-section of the rotor slot. Figure 6 shows the FRFs for the linearised cage-induction and slip-ring machines. The difference between the rotor models changes the shape of the FRF visibly. Because the small-signal parameters of the linearised slip-ring machine are constant in the whole frequency range, based on Fig. 6, one can assume that for the cage-induction machine they are frequency-dependent.

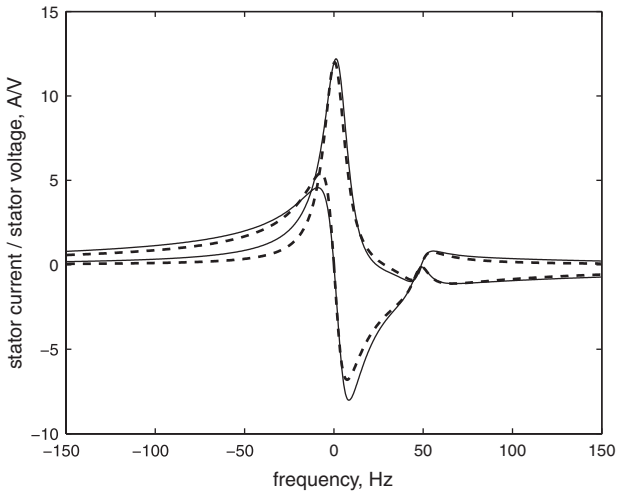

Fig. 6 *FRFs of linearised cage-induction machine (solid line) and linearised slip-ring machine (dashed)*

3.4 Estimation algorithm

The parameters are estimated by minimising the error between the simulated FRF and the FRF given by model (5). The cost function I is defined as

$$I = \sum_{n=1}^{N} \left(\text{Re}\{y_m^n\} - \text{Re}\{y_e^n\}\right)^2 + \left(\text{Im}\{y_m^n\} - \text{Im}\{y_e^n\}\right)^2 \quad (12)$$

where n is the index and N is the length of the data vector. Subscript m refers to the FRF obtained from the impulse method and subscript e refers to the FRF from model (5) with parameter estimates.

Evolutionary algorithms have become the most widely applied methods in a large variety of optimisation problems. The main advantage of an evolutionary algorithm is that the form of the cost function can be arbitrary since the algorithm only needs the value of the function, not the derivatives. Here, a method called 'differential evolution' has been chosen. It has been proved to be fast and robust in multivariable search [20]. All five parameters cannot be identified unequivocally from the external data using global optimisation [2], so the optimisation problem is constricted assuming the stator and rotor leakage inductances to be equal.

4 Results

4.1 Impedance method

First, the steady-state parameters of the cage-induction and slip-ring machine were calculated using the impedance method. The results are given in Table 2. The parameters were also calculated at different values of the supply voltage and slip. Figures 7 and 8 show that the values of the rotor resistance and rotor leakage reactance ($f_s = 50$ Hz) vary significantly with the slip.

Table 2: Steady-state parameters calculated using impedance method

	Cage	Slip-ring
	$s = 2\%$	$s = 2\%$
R_s [Ω]	0.08357	0.08357
$X_{\sigma s}$ [Ω]	0.2476	0.2477
X_m [Ω]	8.431	8.350
$X_{\sigma r}$ [Ω]	0.4815	0.4729
R_r [Ω]	0.06681	0.06684

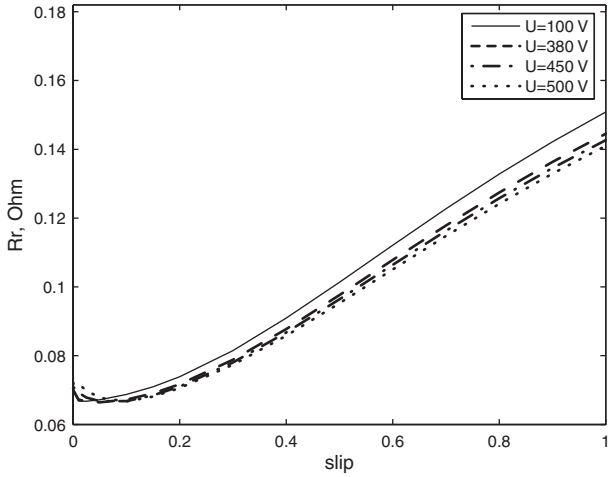

Fig. 7 *Variation of rotor resistance along with the supply voltage and slip*

4.2 Impulse response test

First, the parameters of the linearised FE models are estimated. The FRF of the linearised slip-ring machine is fitted to model (5) using the whole frequency range -200 to 200 Hz since the parameters are independent of frequency. The FRF of the linearised cage-induction machine is fitted so that the stator resistance is fixed to the value of the FE model to simplify the problem. The frequency range is limited to 49.5–50.5 Hz in order to find the parameters related to the rated operation point, since the rotor quantities are likely to vary along with the frequency. Zero padding is used to obtain a resolution of 0.01 Hz.

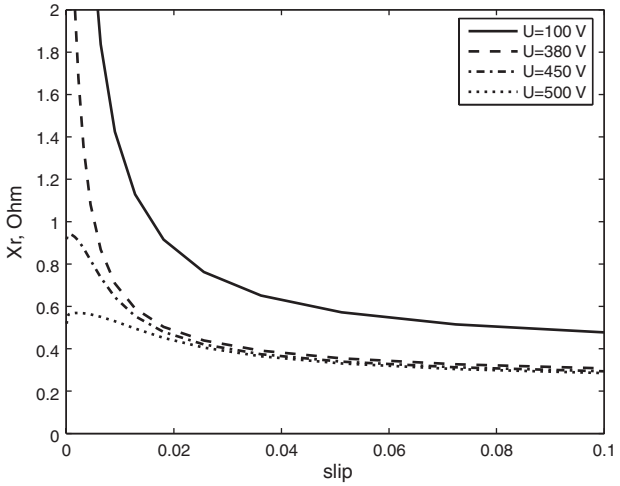

Fig. 8 *Variation of rotor leakage reactance against supply voltage and slip*

Similar estimation procedures are performed for the nonlinear slip-ring and cage-induction machines. The accuracy of the fit is evaluated calculating the average relative error:

$$e_{\text{ave}} = \frac{\sum_{n=1}^{N} \frac{\left|\text{Re}\{y_m^n\}\right| - \left|\text{Re}\{y_e^n\}\right|}{\left|\text{Re}\{y_m^n\}\right|} + \sum_{n=1}^{N} \frac{\left|\text{Im}\{y_m^n\}\right| - \left|\text{Im}\{y_e^n\}\right|}{\left|\text{Im}\{y_m^n\}\right|}}{2N} \tag{13}$$

About 50 iterations are needed to find the minimum of (12). The parameters obtained for the small-signal model are given in Table 3. The reactances are calculated from the estimated inductance values using a supply frequency of 50 Hz.

The small-signal parameters were also estimated by fixing the ratio between the leakage inductances to the ratio given by the impedance method (Table 2). With this assumption, the fit is equally accurate and the performance of the model remains the same. The sum of the leakage inductances and the value for the magnetising inductance increase by 2%. The value of the rotor resistance increases by 2–4.7%. The largest increase occurs in the nonlinear cases.

Next, the parameters of the cage-induction machine were estimated piecewise for the range –150 to 150 Hz similarly as for the rated load at 50 Hz. For the leakage inductance, a reasonable value was found quite rapidly almost in the whole range studied. In the range -20 to 20 Hz and around 100 Hz, finding the minimum takes 2000–3000 iterations. The same regions are also problematic for the

Table 3: Small-signal model parameters estimated from FRF

	Slip-ring linear	Cage linear	Slip-ring nonlinear	Cage nonlinear
r_s [Ω]	0.08370	0.08357 (fixed)	0.0842	0.08357 (fixed)
x_σ [Ω]	0.2902	0.2510	0.2526	0.34831
x_m [Ω]	7.3753	7.665	3.3503	4.2863
r_r [Ω]	0.06700	0.06710	0.06661	0.07511
e_{ave} [%]	3.1	0.07	5.1	1.9

magnetising inductance, which has several values giving almost the same fitting error. Model (5) is not so sensitive to the value of the magnetising inductance since only about 10% of the stator current flows through the magnetising branch. Nevertheless, the fit is very accurate. The relative error between the simulated FRF point and the FRF point calculated from the parameter estimates varies between 0.005 and 0.08%.

The values of both the magnetising inductance and the leakage inductance have a maximum at 50 Hz. The rotor resistance has a minimum between 45 and 50 Hz. The estimated rotor resistance is shown in Fig. 9.

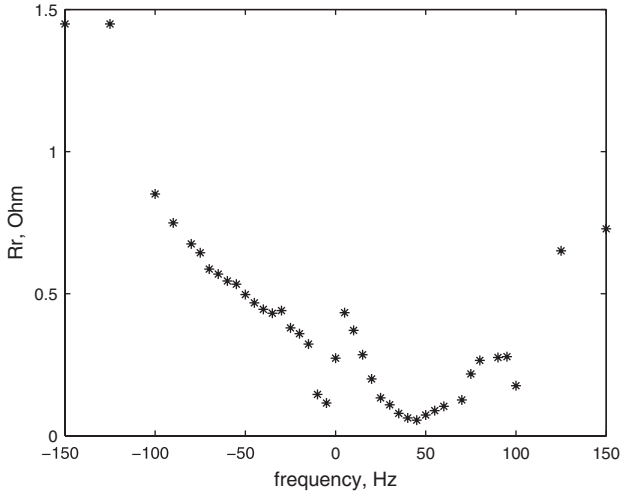

Fig. 9 *Small-signal rotor resistance of cage-induction machine*

4.3 Measurements

4.3.1 Measurement of steady-state parameters: The steady-state parameters were also estimated from the results measured in a temperature-rise test. The stator quantities were measured using a power analyser, the mechanical ones with a torque transducer. The machine was first run at the rated load to a thermal equilibrium. After reaching a steady state, the load was stepwise reduced by 10%. A series of 20 measurements was made just before the load change and another one immediately after the load change. A similar sequence of measurements was repeated when the load was increased by 10%. The measurement results are given as average values in Table 4.

The parameters were estimated using the results of the impedance method (Table 3, column 1) as initial values. The rotor resistance, stator leakage reactance and magnetising reactance were varied according to (14):

$$R_r^n = 0.75R_{r0} + \sum_{n=1}^{200} n\frac{0.5R_{r0}}{200} \tag{14}$$

Table 4: Measurements of temperature-rise test

	Meas. 1	Meas. 2	Meas. 3	Meas. 4
U_s [V]	380.1	380.5	380.1	379.6
I_s [A]	70.07	64.54	70.84	77.08
cosφ	0.8511	0.8428	0.8519	0.8580
T_e [Nm]	237.7	217.3	240.6	262.9
s [%]	1.997	1.799	2.024	2.248

The ratio between the leakage inductances was calculated from the initial values and the stator resistance was constant. Using all the combinations of the parameters, the stator current and electromagnetic torque were calculated and compared with the measured values. The parameter values that minimise the total square error are given in Table 5.

Table 5: Measured steady-state parameters

R_s [Ω]	0.08357
$X_{\sigma s}$ [Ω]	0.2353
X_m [Ω]	8.263
$X_{\sigma r}$ [Ω]	0.4609
R_r [Ω]	0.06564

4.3.2 Measurement of FRF with harmonic excitation: Some points from the FRF were measured using the harmonic excitation to validate the simulated FRF. The 37 kW motor was fed from a 50 Hz, 750 kVA synchronous generator and run at the rated load long enough to reach the thermal steady state. A harmonic, three-phase excitation voltage was taken from a variable frequency, 150 kVA synchronous generator and injected to the supply line of the 37 kW test motor via a three-phase current transformer. The measurement setup is shown in Fig. 10.

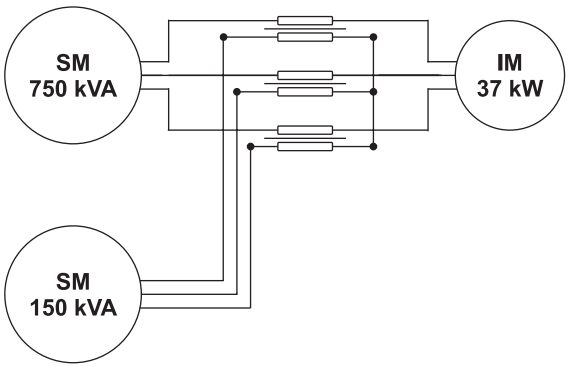

Fig. 10 *Measurement setup for harmonic excitation*

The frequencies injected one by one were 10, 15, 20, 25, 75, 100, 125, 150, 200, 250 Hz, and both the negative and positive phase sequence was applied. Four different excitation amplitudes were used at each frequency. These amplitudes ranged from 0.3 to 1.3% of the rated voltage at the lowest frequency, and were between 1.6 and 6.3% at the highest frequencies. The voltages and currents of the test motor were measured and recorded at a 70 kHz sampling frequency using a three-phase power analyser.

The frequency response without the harmonic excitation contains peaks at the supply frequency 50 Hz and at −250 Hz, which is the fifth harmonic produced by the induction machine itself. Changing the excitation amplitude has an effect mainly at the frequencies −20–10 Hz and 10–20 Hz, but there does not exist any clear pattern. In the simulations, the relative amplitude was changed linearly according to the frequency. From the measurements, the closest relative amplitude giving a reasonable result is chosen for the comparison. Table 6 gives the chosen relative amplitudes, and Fig. 11 shows the relative difference between the measured and simulated FRF points. The FRF

Table 6: Relative amplitudes chosen for comparison between measured and simulated FRF points

|Freq.| [Hz]	a_{rel} (meas.)	a_{rel} (sim.)
10	0.3	0.5
15	0.5	0.6
20	0.6	0.7
25	1.6	0.8
75	3.2	1.7
100	4.7	2.2
150	6.3	3.1
200	6.3	4.1
250	6.3	5.0

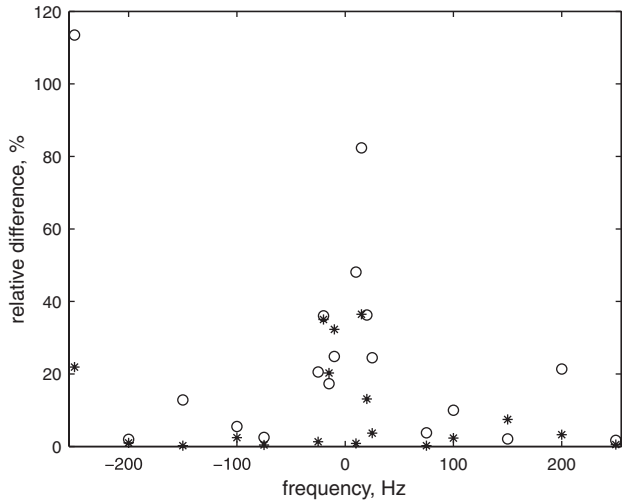

Fig. 11 *Relative difference between measured and simulated FRF points*
○ real part circle
* imaginary

at -250 Hz is distorted by the fifth harmonic, but otherwise the FRFs at higher frequencies correspond to each other relatively well. The real parts at low frequencies deviate the most.

The impulse excitation can be applied to the machine in a similar way as the harmonic excitation. However, the fundamental frequency and slot harmonics should be filtered from the excitation and response signals before calculating the FRF. This problem has not yet been solved.

5 Discussion

5.1 Parameter estimation

Previously, FEA has been used to obtain the steady-state circuit parameters [7–13]. However, small-signal parameters are required for adjusting the control algorithms. In this work, these parameters are obtained from the results of the time-stepping FEA.

The nonlinearity of the core materials and skin effect of the conductors cause problems for small- signal parameter estimation. These factors are not present in the linearised slip-ring motor, and the parameter estimation works well. For the linearised cage-induction motor, the skin effect of the rotor bars is relatively strong and a constant-parameter model is valid only within a narrow frequency range. Dividing the frequency range into short intervals, piecewise constant parameter values can be found. For the linearised machines, the parameters estimated from the numerical impulse test agree well with the steady-state parameters obtained from the impedance method.

The parameter values obtained from the impulse test are related to the incremental permeability. The harmonic analysis of the impedance method utilises an effective permeability and gives related circuit parameters. In a linear material, these two quantities are equal, and equal parameters are to be expected. For a saturated machine, the two methods are expected to give different circuit parameters, especially inductance values. Based on the fundamental difference discussed above, the parameters from the impedance method are valid to model the total RMS currents and voltages. The parameters estimated from the numerical impulse test serve better for the purpose of control.

5.2 Frequency response function

When using voltage impulses, the choice of the impulse magnitude near DC had a significant influence on whether harmful saturation and distortion of the FRF occur. The parameters of the cage-induction machine were estimated using a very narrow frequency range, which makes their values sensitive to the local perturbations in the FRF. If a current impulse is applied instead of voltage, the effect of saturation can be reduced since the admittance at the DC is large. When using voltage impulse 2, the amplitude can be refined so that an excessively high transient in the current can be avoided.

In the harmonic excitation, all the simulated FRF points were synchronised to the supply voltage. In the measurements, this is the case only at ± 25 and ± 100 Hz. The basic simplification of the two-dimensional FE analysis is that it cannot model the core losses or the skin effect in steel laminations and stator conductors. Even so, the simulated and measured FRF points are relatively close to each other within the ranges -250 to -25 Hz, and 25 to 250 Hz.

In the performed simulations, one impulse response test took about seven hours since 40 000 time steps were computed. If only the first 10 000 time steps and zero padding are used to obtain the FRF with the same frequency resolution, the parameters at 50 Hz differ from the first ones in the third decimal place. When using less than 5000 time steps the shape of the FRF becomes distorted. Shortening the simulations may become especially useful, when a wider frequency range is studied. For example, with the impulse length 1.0 ms, the frequency range is expanded to -2000 to 2000 Hz. To obtain the same amount of data from the impulse, the step size of the FE analysis has to be reduced to 10 μs and the total simulation time becomes five times longer.

5.3 Continuation

If the skin effect in the rotor bars is included in the FE model the rotor parameters vary along with the frequency. Then, the basic circuit model with constant parameters is sufficient only for a narrow frequency range, representing only one operation point. In future, a more advanced analytical model capable of including the skin effect will be looked for. The impulse response test will also be developed further in order to minimise the nonlinear behaviour of the machine. The impulse test will also be performed by measurement.

6 Conclusions

The applicability of the numerical impulse response test in estimation of the small-signal model parameters has been studied. Because of the nonlinear nature of the electrical machine, the choice of the excitation signal is very important. In the case of the slip-ring machine, the parameter extraction for a wide frequency range was successful. The parameters of the cage-induction machine are frequency-dependent and they had to be estimated piecewise for one operation point at a time. Saturation can create additional frequency components and therefore the piecewise estimation is more sensitive to local flaws in the frequency response data. Even so, reasonable parameter values can be found also for the cage-induction machine.

7 References

1 Velez-Reyes, M., Minami, K., and Verghese, G.C.: 'Recursive speed and parameter estimation for induction machines'. Proc. IEEE Ind. App. Society Annual Meeting, San Diego, CA, USA, 1989, pp. 607–611

2 Corcoles, F., Pedra, J., Salichs, M., and Saintz, L.: 'Analysis of induction machine parameter identification', *IEEE Trans. Energy Convers.*, 2002, **17**, (2), pp. 183–190

3 Ursem, R.K., and Vadstrup, P.: 'Parameter identification of induction motors using differential evolution'. Proc. IEEE Congress on Evolutionary Computation (CEC), Canberra, Australia, 2003, pp. 790–796

4 Holliday, D., Green, T.C., and Williams, B.W.: 'On-line measurement of induction machine stator and rotor winding parameters'. Proc. Fifth IEE Int. Conf. on Power Electronics and Variable-Speed Drives, London, 1994, pp. 465–469

5 Jansen, P.L., and Lorenz, R.D.: 'Transducerless position and velocity estimation in induction and salient AC machines', *IEEE Trans. Ind. Appl.*, 1995, **31**, (2), pp. 240–247

6 Holtz, J.: 'Sensorless control of induction machines – with or without signal injection?', *IEEE Trans. Ind. Electron.*, 2006, **53**, (1), pp. 7–30

7 Williamson, S., and Begg, M.C.: 'Analysis of cage induction motors – a combined fields and circuits approach', *IEEE Trans. Mag.*, 1985, **MAG-21**, (6), pp. 2396–2399

8 Williamson, S., Lim, L.H., and Robinson, M.J.: 'Finite-element models for cage induction motor analysis', *IEEE Trans. Ind. Appl.*, 1990, **26**, (6), pp. 1007–1017

9 Arkkio, A.: 'Analysis of induction motors based on the numerical solution of the magnetic field and circuit equations' (Electrical Engineering Series, No. 59, Acta Polytechnica Scandinavica, Helsinki, 1987), p. 97, available: http://lib.tkk.fi/Diss/198X/isbn951226076X/

10 Dolinar, D., De Weerdt, R., Belmans, R., and Freeman, E.M.: 'Calculation of two-axis induction motor model parameters using finite elements', *IEEE Trans. Energy Convers.*, 1997, **12**, (2), pp. 133–142

11 Bianchi, N., Bolognani, S., and Comelato, G.: 'Finite element analysis of three-phase induction motors: comparison of two different approaches', *IEEE Trans. Energy Convers.*, 1999, **14**, (4), pp. 1523–1528

12 Papazacharopoulos, Z.K., Tatis, K.V., Kladas, A.G., and Manias, S.N.: 'Dynamic model for harmonic induction motor analysis determined by finite elements', *IEEE Trans. Energy Convers.*, 2004, **19**, (1), pp. 102–108

13 Kanerva, S., Seman, S., and Arkkio, A.: 'Inductance model for coupling finite element analysis with circuit simulation', *IEEE Trans. Magn.*, 2005, **41**, (5), pp. 1620–1623

14 Tenhunen, A.: 'Electromagnetic forces acting between the stator and eccentric cage rotor'. Doctoral thesis,Laboratory of Electromechanics, Helsinki University of Technology, Report 69, Espoo2003 p. 40, available: http://lib.tkk.fi/Diss/2003/isbn9512266830/

15 Holopainen, T.P.: 'Electromechanical interaction in rotordynamics of cage induction motors' (VTT Publications 543, Espoo, 2004), p. 64, available: http://lib.tkk.fi/Diss/2004/isbn9513864057/

16 Luomi, J., Niemenmaa, A., and Arkkio, A.: 'On the use of effective reluctivities in magnetic field analysis of induction motors fed from a sinusoidal voltage source'. Proc. Int. Conf. on Electrical Machines, Technische Universität München, Germany, 1986, Vol. 2, pp. 706–709

17 Smith, A.C., Healey, R.C., and Williamson, S.: 'A transient induction motor model including saturation and deep bar effect', *IEEE Trans. Energy Convers.*, 1996, **11**, (1), pp. 8–15

18 Sudhoff, S.D., Aliprantis, D.C., Kuhn, B.T., and Chapman, P.L.: 'An induction machine model for predicting inverter-machine interaction', *IEEE Trans. Energy Convers.*, 2002, **17**, (2), pp. 203–210

19 Ewins, D.J.: 'Modal testing: theory, practice and application' (Research Studies Press Ltd., Hertforshire, UK, 2000, 2nd edn.)

20 Storn, R.: 'On the usage of differential evolution for function optimization'. Proc. IEEE Biennial Conf. of the North American Fuzzy Information Processing Society, Berkeley, CA, USA, 1996, pp. 519–523